Tectonophysics 747–748 (2018) 40–53

Contents lists available at ScienceDirect

Tectonophysics

journal homepage: www.elsevier.com/locate/tecto

Earthquake geology of the last millennium along the Boconó Fault, Venezuela

Lea Pousse-Beltran[a,c,*], Riccardo Vassallo[a], Franck Audemard[b], François Jouanne[a], Javier Oropeza[b], Stéphane Garambois[a], Jelime Aray[b]

[a] Université Grenoble-Alpes, Université de Savoie Mont-Blanc, CNRS, IRD, IFSTTAR, ISTerre, 38000 Grenoble, France
[b] Venezuelan Foundation for Seismological Research, FUNVISIS, El Llanito, Caracas 1070, Venezuela
[c] Aix-Marseille Université, CEREGE, CNRS-IRD UMR 34, Aix-en-Provence, France

ARTICLE INFO

Keywords:
Earthquake geology
Active tectonics
Yaracuy Valley, Venezuela

ABSTRACT

The Holocene tectonic activity of Latin American countries is poorly constrained because of the short time span of the instrumental record and the lack of any seismic calendar during pre-colonization times. Therefore, some areas with low and diffused seismicity have been catalogued as a "seismic gap". It has been suggested that the northernmost segment of the Boconó Fault in Venezuela is one of these areas, although a recent MW 7.4 event that occurred in 1812 has been well documented by a historical investigation. In this study, we mapped the historical events triggered by the Boconó Fault using a paleoseismological investigation, a geological interpretation of high-resolution satellite images, field mapping as well as ground-penetrating radar (GPR) profiles at selected trench sites. Our results suggest that at least three seismic events had produced surface ruptures in the trench site based on the exposed trench stratigraphy as well as the results of radiocarbon dating and age models: i) a latest event (E3) that occurred between 1545 and 1825 CE, ii) a previous event (E2) that occurred between 1483 and 1743 CE and iii) an older event (E1 before 1456–1636 CE). The E3 event might correspond to the 1812 major earthquake. These results further support the fact that the 1812 event was triggered by the Boconó Fault and that the rupture reached the surface. The potential slip deficit along the studied segment ranges from 1.7 to 2.3 m and corresponds to Mw ~7, assuming that the 1812 CE earthquake released all of the strain stored earlier. As the time span between events E2 and E3 is short (< 360 years), it is worth to pay a great attention to the seismic risk assessment for a densely inhabited Boc-e fault segment.

1. Introduction

In Latin American countries, the historical seismicity record is quite brief: from the time of Spanish colonization until the present day. In Venezuela particularly, it is restricted to after the 3rd trip of Columbus to the New World, who reached its eastern coasts in 1498 CE. During the last ~500 years of the historical seismicity record, major Quaternary faults have been reactivated at least once or at most twice (Audemard, 2014). However, the history of these last 500 years is still under debate due to the scarcity of archives and thus difficulties to ascribe a historical event to a fault. Paleoseismological studies allow researchers to ascribe events and to enlarge the temporal window into the past, revealing the last 10^0 to 10^4 years of main fault activity. Since these events are associated with $M_W \geq 7$ and occurred in populated areas, it is therefore necessary to know the calendar of the fault activity during the Holocene so as to assess the seismic hazard. From these considerations, we excavated a trench across the Boconó Fault, a main strike slip fault extending 500 km and comprising five segments. We studied the segment that crosscuts the Yaracuy valley, where on March 26, 1812 a M_{WI} 7.4 destructive event occurred (Choy et al., 2010; Altez, 2016). Although this event was well reported, this area is considered as a "seismic gap" due to the low and diffuse instrumental seismicity recorded since 1910 (Audemard, 2002). Several faults, likely active, crosscut this valley and might trigger this event, but along this segment of the Boconó Fault only two trenches were carried out (Audemard, 2016), and the 1812 event was documented in one of these trenches. Apart from this event, no other event has been identified since 1200 BCE, conversely to other Boconó Fault segments (Audemard, 2014

* Corresponding author.
E-mail addresses: pousse@cerege.fr (L. Pousse-Beltran), riccardo.vassallo@univ-smb.fr (R. Vassallo), faudemard@funvisis.gob.ve (F. Audemard), francois.jouanne@univ-smb.fr (F. Jouanne), joropeza@funvisis.gob.ve (J. Oropeza), Stephane.Garambois@univ-grenoble-alpes.fr (S. Garambois), jaray@funvisis.gob.ve (J. Aray).

https://doi.org/10.1016/j.tecto.2018.09.010
Received 11 January 2018; Received in revised form 14 September 2018; Accepted 18 September 2018
Available online 26 September 2018

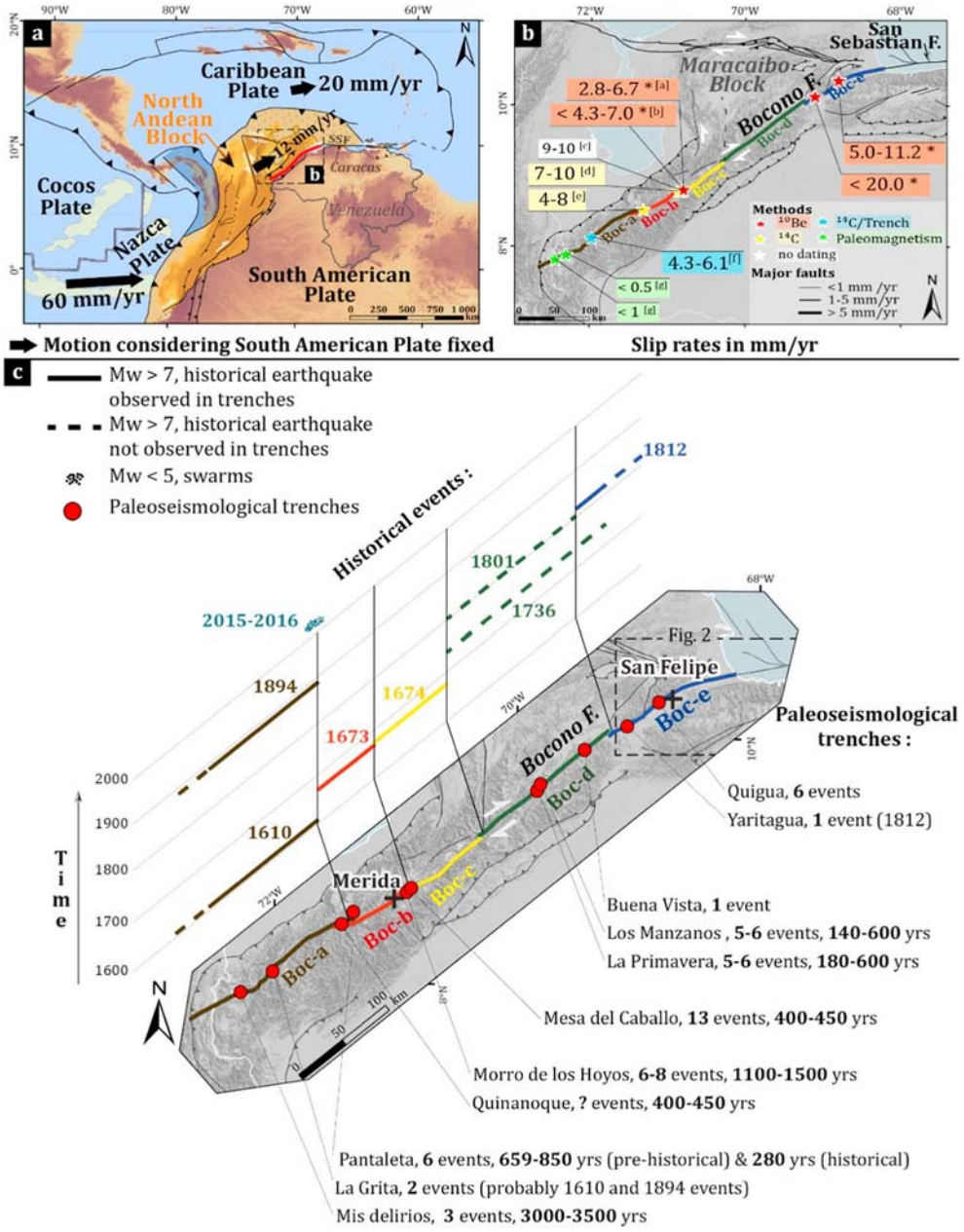

Fig. 1. A) Geodynamic context of Venezuela. The North Andean Block (in yellow), composed of minor blocks, accommodates part of the relative displacement between the South American, Nazca and Caribbean plates. The Boconó Fault is shown in red, SSF is the San-Sebastian Fault. This figure is based on Trenkamp et al. (2002), DeMets et al. (2010), Egbue and Kellogg (2010) and Monod et al. (2010). B) Quaternary slip rates of the Boconó Fault (Pousse-Beltran et al., 2017). The color lines highlight the five segments of the fault based on Audemard et al. (2000). The slip rate references quoted are: [a] Wesnousky et al. (2012), [b] Wesnousky et al. (2012) and Carcaillet et al. (2013), [c] Giegengack et al. (1976) and Egbue and Kellogg (2010), [d] Audemard et al. (1999); [e] Soulas (1986), [f] Audemard (1997), [g] Singer and Beltran (1996). C) Spatio-temporal distribution of the historical seismicity and location of the trench sites carried out along the Boconó Fault (modified after Audemard (2014)). This figure summarizes the fault segment characteristics: historical events, trench sites, number of events dated in the trenches and return period. References are for the "Mis Delirios" and "La Grita" trenches: Audemard (1997, 1998), for the "Quinanoque" and "Pantaleta" trenches: Alvarado et al. (2008), for the "Morro de los Hoyos" trench is Audemard et al. (1999), for the "Mesa del Caballo" trench is Audemard et al. (2008), for the "La Primavera" and "Los Manzanos" trenches is: Audemard (2008), for the "Buena Vista" trench is Beltran et al. (1990), and finally for the "Quigua" and "Yaritagua" trenches is Audemard (2016). See Fig. S1 in the supplementary material for the detailed chronology of the events dated in the trenches. (For interpretation of the references to color in this figure legend, the reader is referred to the web version of this article.)

and references therein). Since InSAR analysis shows no aseismic slip along the fault (Pousse-Beltran et al., 2017), the regional deformation should be accommodated seismically if no slow slip event occurred. Considering the minimum Quaternary velocity estimated in this area, 5.0 mm·a^{-1} (Pousse-Beltran et al., 2017), this implies that between 1812 and 1200 BCE, there is a slip deficit minimum of ~15 m. This important deficit should be accommodated by several earthquakes, which may indicate that a significant part of the paleoseismological calendar is missing. Consequently, the purpose of our manuscript is to: 1) improve the Holocene activity calendar of the northernmost Boconó Fault segment, and 2) ratify the occurrence of the destructive 1812 event on this fault segment.

2. Geological setting

2.1. Quaternary active tectonics setting

The geodynamics in the southern limit of the Caribbean Plate result from the interaction of three tectonic plates: the South American, Caribbean and Nazca Plates (Freymueller et al., 1993; Trenkamp et al., 2002) (Fig. 1-a). Within this complex plate boundary, Pennington (1981) defined the North Andean Block as a wide zone composed of minor blocks and active faults (Kellogg et al., 1995; Trenkamp et al., 2002; Egbue and Kellogg, 2010). There is a general agreement in geodetic studies that in Venezuela, the North Andean Block (comprising the Triangular Maracaibo Block) escapes to the NNE at an average velocity of ~12 mm·yr^{-1} with respect to the stable South American Plate (Pérez et al., 2011; Reinoza, 2014; Symithe et al., 2015).

In Venezuela, between the Northern Andean Block and the South American Plate lies the NE – SW Boconó Fault system, whose right-lateral strike-slip motion (the Boconó Fault) together with sub-parallel thrust faults, accommodate part of the regional transpressional tectonics (Colletta et al., 1997; Audemard and Audemard, 2002; Audemard, 2005; Pérez et al., 2011; Dhont et al., 2012). The right-lateral strike-slip Boconó Fault described by numerous geologists (Rod, 1956; Bellizzia et al., 1976; Giraldo, 1985; Soulas, 1986; Ferrer, 1991; Beltran, 1994; Audemard, 2005; Audemard, 2009) has been divided into five segments (Boc-a, Boc-b, Boc-c, Boc-d and Boc-e (Audemard

et al., 2000), see Fig. 1-b).

Fig. 1-b summarizes the Quaternary slip rate estimations along the Boconó Fault, whose rates range from 0.5 to 20 mm·yr^{-1}. Four of them are based on < 20 ka offset moraines in the central part of the Boconó Fault dated by Carbon-14 (^{14}C) (Salgado-Labouriau et al., 1977; Soulas, 1986; Audemard et al., 1999) or by Beryllium-10 (^{10}Be) (Wesnousky et al., 2012; Carcaillet et al., 2013; Pousse-Beltran et al., 2017). A fifth slip rate has been estimated in a paleoseismologic trench (Audemard, 1997) along the Boc-a segment. In the Yaracuy Valley, based on ^{10}Be dating and offset alluvial fans, two very recent Pleistocene rates have been estimated at 5.0–11.2 mm·yr^{-1} and < 20 mm·yr^{-1}, respectively (Pousse-Beltran et al., 2017).

Along this 500 km long fault, among the eleven trenches carried out (Fig. 1-c), seven trenches can be used to estimate an average return period (Beltran et al., 1990; Audemard, 1997, 1998, 2008, 2016; Audemard et al., 1999, 2008; Alvarado et al., 2008). Among these studies, a short return period of < 600 years was determined for four southern segments (in five trenches), and a much larger period for the Boc-e segment studied in this contribution.

2.2. Historical events

From the analysis of historic archives (e.g., Cluff and Hansen, 1969; Altez, 2006), the application of Bakun and Wentworth's method for estimating intensities (Bakun and Wentworth, 1997; Palme et al., 2005; Choy et al., 2010) and paleoseismological studies (Audemard, 2014 and references therein), it was concluded that each of the segments of the Boconó Fault has triggered at least one Mw ≥ 7 historical earthquake since 1600 (Audemard, 2014, 2016) (Fig. 1-c). Based upon these historical events, Audemard (2014) proposed that along the Boconó Fault the rupture propagates from south-west to north-east following the geometrical segmentation (Fig. 1-c). The geometrical discontinuities that limit the five main segments, according to this author, could be barriers to rupture propagation. However, this hypothesis is only based on the last seismic cycle corroborated by historical seismicity and paleoseismicity.

Among the most destructive events, the March 26, 1812 earthquake caused severe damage from Merida to Caracas, especially in the Yaracuy Valley (Altez, 2006; Choy et al., 2010) This earthquake was associated with several ruptures (Fiedler, 1961, 1972; Centeno Graü, 1969; Audemard, 2002; Altez, 2006, 2016). Two main studies have characterized these ruptures: i) Choy et al. (2010) using the methodology described by Bakun and Wentworth (1997) based on individual intensity observations and ii) Altez (2005a, 2005b) who studied the historical archives. These two contributions showed that the 1812 event was composed of three sub-events (Fig. 2-a).

1) At around 4 pm on March 26, 1812, a first rupture occurred, which destroyed the city of San Felipe (in the Yaracuy Valley), with an estimated M_{WI} 7.4 ± 0.35 (M_{WI} magnitude determined using intensities and calibrated with moment magnitudes; Choy et al. (2010)) and a main epicenter located near 10.20°N 68.95°W. These authors also proposed that the rupture propagated over a length of 90 to 100 km along the Boconó Fault (segment Boc-e). This statement seems to be confirmed by the archives collected by Altez (2005b) which provided evidence that the rupture reached the surface since open cracks and offset drainage were reported. Audemard (2016), in a paleoseismological trench carried out near Yaritagua, determined that the 1812 event occurred in association with Boc-e (cf. Section 2.3 and Fig. 2-b).
2) A second rupture occurred and destroyed the capital city of Venezuela, Caracas. For this second event, Choy et al. (2010) estimated a M_{WI} 7.1 ± 0.33 with an epicenter located at 10.60°N, 67.10°W. They stated that the rupture propagated over 70 km and that it occurred along the San Sebastian Fault, an offshore fault located in the continuity of the Boconó Fault.
3) One hour later (around 5 pm) after these main events, a localized earthquake occurred in Merida (Mw 5.6–6.0) at 350 km from San Felipe (Rodriguez and Audemard, 1997; Laffaille and Ferrer, 2003; Palme et al., 2005). This event has not yet been correlated with a particular fault, likewise the link with this subevent and the two main subevents (above) remains unclear.

Given that the archives reported that the subevents in San Felipe and near Caracas occurred at the same time or probably just several minutes apart, it has been proposed that there is a relationship between the two (Audemard, 2002; Choy et al., 2010). However, as there is no archive stating which rupture occurred first, we cannot exclude that the rupture may have propagated ~380 km from Barquisimeto (southern tip of the Boc-e segment) to Caracas (near the San Sebastian Fault, Fig. 2).

Another seismic event was documented in 1736. Martinez Silva et al. (2016) documented three churches damaged by this event in the cities of Barquisimeto, Santa Rosa del Cerrito and Guama (Fig. 1 and Fig. 2). These towns are located near the Boconó Fault. However, the intensity data gathered so far has been insufficient to make a proper intensity map in order to derive a magnitude estimate.

2.3. Previous paleoseismological studies in the Boc-e segment (Yaracuy Valley)

Along this fault segment, two trenches were carried out by Audemard (2016). From west to east they are called the Yaritagua trench (N10°06′11.8″, W69°05′48.3″) and the Quigua trench (N10°17′55.1″ W68°51′18.2″) (red triangles in Fig. 2-b and Figs. S7, S8 in the Supplementary material). The Yaritagua trench was excavated in the eastern prolongation of a north facing fault scarp, in which Audemard (2016) identified an event through a filled open crack that reaches the modern surface soil. The open crack affects aligned pebbles dated between 1450 and 1650 CE. This date corresponds to the minimum age of the latest deformation. The organic material in the crack was dated between 1520 and 1950 CE Consequently, the author attributes the open crack to the 1812 event. In the Quigua trench site, the fault is divided into two parallel traces crosscutting an alluvial fan (Audemard, 2016). Excavation was carried out across the SE trace which exhibits a SW facing scarp. Trench logs show faulted conglomerate deposits (fluvio-torrential deposits), aligned pebbles, colluvial wedges and open cracks indicating the succession of several ruptures. Based upon the trench logs and radiocarbon ages, Audemard (2016) observed a succession of 6 to 8 events that occurred between 20 ka and 1 ka B.C.E.

From these two trench analyses, Audemard (2016) concluded that the time interval between events oscillates between 1500 and 5000 years and that the average return period ranges from 2500 to 3000 years (which corresponds to the time interval between the two last events). The minimum Quaternary slip velocity estimated in this area is 5.0 mm·a^{-1} (Pousse-Beltran et al., 2017) which implies a potential slip accumulation of 7.5 to 25 m between these time intervals. Several earthquakes are missing and therefore, as proposed by Audemard (2016), part of the deformation is missing in the Quigua trench due to one or any combination of the following factors:

- Erosion induced by debris flow events, partially removing previous events of the same nature (incomplete sedimentary record),
- Absence of sediment yield since the alluvial fan was disconnected from the catchment outlet,
- Difficulties to identify stratifications in conglomeratic deposits,
- Slow transport deposit processes disabling colluvial wedge formation,
- Deformation distribution on the parallel fault trace located to the NW, or on another unmapped fault trace.

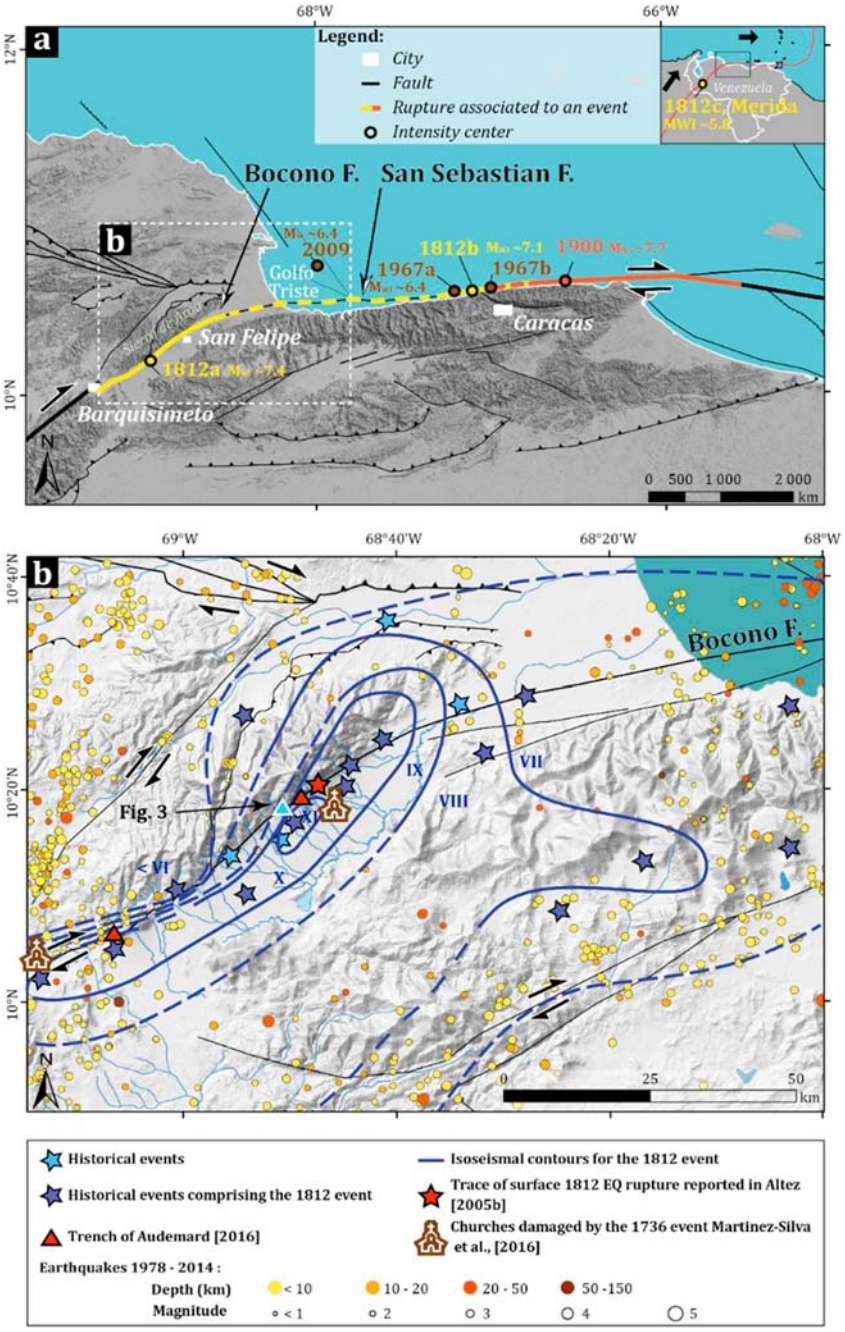

Fig. 2. A) Sub-events and epicenters associated with the 1812 event. The yellow line marked as 1812a corresponds to the rupture inferred along the Boc-e segment which destroyed the cities of Barquisimeto and San Felipe. The yellow line demarcated as 1812b corresponds to the rupture along the San Sebastian Fault which destroyed Caracas. The yellow dot denoted as 1812c in the right top frame is the localized event that occurred near the city of Merida (Choy et al., 2010). The dotted yellow line represents the possible rupture between the 1812a and 1812b events in the case of a continuous rupture. The ruptures and epicenters of the 1900 and 1967 events are drawn following Audemard (2002), Choy et al. (2010) and Colón et al. (2015). The fault mapping is based on Audemard et al. (2000). B) Seismo-tectonic context of the Yaracuy Valley. The stars represent cities where an earthquake has been reported since 1802, the filled purple stars correspond to cities where the 1812 event was felt most strongly (Casas-Sainz, 1991; Choy et al., 2010). The purple lines represent isoseismal contours extrapolated from the intensity reported in the cities (stars on the map) in 1812 and the isoseismal map in Altez (2016). The dots represent the instrumental seismicity recorder by FUNVISIS and the International Seismological Center (2013) between 1978 and 2014. The blue and white triangle indicates the trench site studied in this contribution. (For interpretation of the references to color in this figure legend, the reader is referred to the web version of this article.)

The missing part of the deformation in the trench can also be used to explain: (i) the absence of the 1812 Mw > 7 event and (ii) a long return period compared to the other Boconó Fault segments (Fig. 1-c). The paleoseismological calendar derived from these two trench studies carried out by Audemard (2016) is therefore incomplete. It is then necessary to carry out other trenches along the Boc-e segment. Therefore in this contribution, we propose a new paleoseimological study in order 1) to further confirm the Holocene activity of this Boconó Fault segment, 2) to identify historical events in the trench record, and 3) to ratify the ascription of the 1812 event to the segment and to constrain the 1812 CE rupture extension.

3. Study site and methods

3.1. Site

The trenching site (10°16′24″N, 68°52′56″W, altitude of ~636 m) is located near the La Gotera village on a road that leads to the Higuerón village. The site is located 3–4 km from the Quigua trench. Toward the SW, the main fault trace crosscuts the Neoproterozoic-Paleozoic gneiss of Yaritagua (Nevado, 2012). This main trace offsets several drainages and is observed through a 6–8 m high scarp. Toward the NE, the main fault trace exhibits several 50 to 100 m long shutter ridges. These features laterally divert drainages by several tens of meters and attest to the major dextral

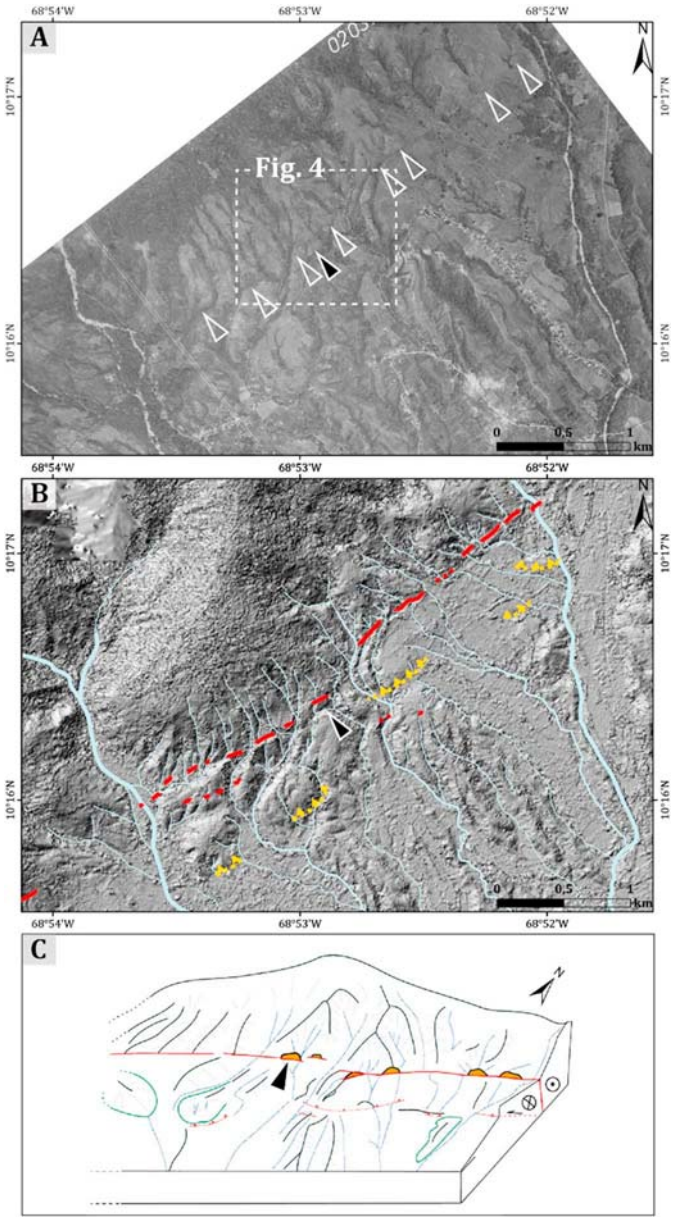

Fig. 3. Mapping of the Boconó Fault in the trenching site (black arrow). A) Aerial photograph (1:35000, No. 144 – mission 020317), the white arrows show the morphological markers of the fault's activity (shutter ridge, fault scarp). To the NW of the trenching site, several drainages are offset. B) DEM shaded (light at the N0, azimuth 45°). The red lines represent the principal fault trace characterized by a dextral component. The dashed yellow lines indicate parallel fault traces with a reverse component. The DEM has been constructed with two Pleiades images at a resolution of 50 cm with the AMES-Stereo Pipeline software (Moratto et al., 2010). The DEM is also shown in the supplementary material (Fig. S2) without interpretation. C) Block diagram of the studied zone; the crests, drainages and fault trace are represented, respectively, in black, blue and red. The shutter ridges are shown in orange. (For interpretation of the references to color in this figure legend, the reader is referred to the web version of this article.)

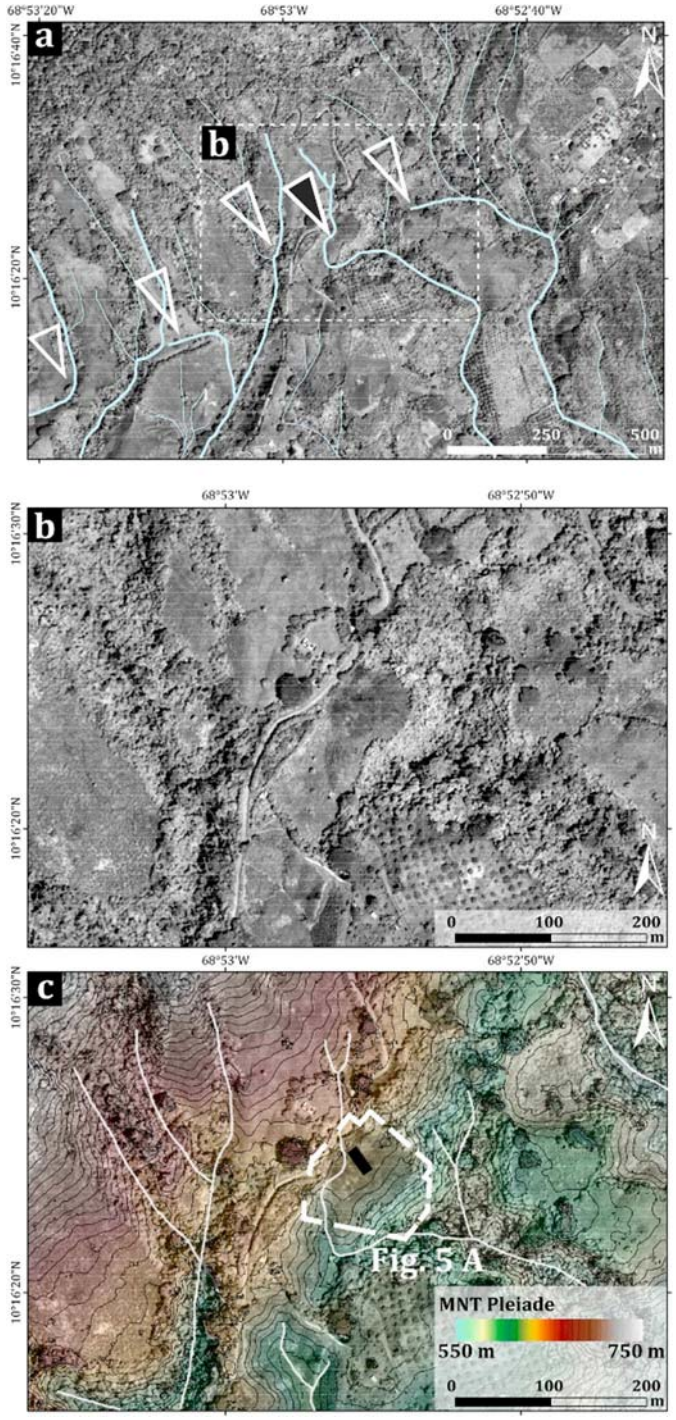

Fig. 4. Pleaides images at a resolution of 50 cm in the trenching site. A) Morphological markers (shutter ridges, fault scarp) indicating the Boconó Fault trace (shown by white arrows). The trenching site is indicated by the black arrow. The image is a Pleiades image at a resolution of 50 cm. B) Zoom on the trenching site. C) Same image, the black rectangle represents the excavation and white lines indicate the drainages. The DEM constructed with two Pleiades images is transparent in color and the elevation contours, spaced 5 m apart, are represented by black lines.

component of the fault. Southward, a minor branch parallel to the previous trace shows a reverse component that creates a meter-scale scarp. (Fig. 3 and Fig. 4-a). The area is not known for being concerned by ice glaciers during cold periods. In Venezuela, glacier advances have been documented at an altitude of at least 2600 m in the Early Merida Glaciation (~60–90 ka) and during the Last Glacial Maximum (LGM) (Ceballos and Angel, 2016; Kalm and Mahaney, 2011; Schubert, 1974).

The trenching site corresponds to a shutter ridge oriented N75°. The shutter ridge chosen for the excavation is ~70 m long and 1.50 m high. It offsets a gully by ~40 m and creates a pond (Fig. 4-b–c and Fig. 5). The drainage supplies centimetric to decimetric clasts, originating from the schists (Fig. 5-b) in the Paleozoic formation known as the Yaritagua Complex (Hackley et al., 2005).

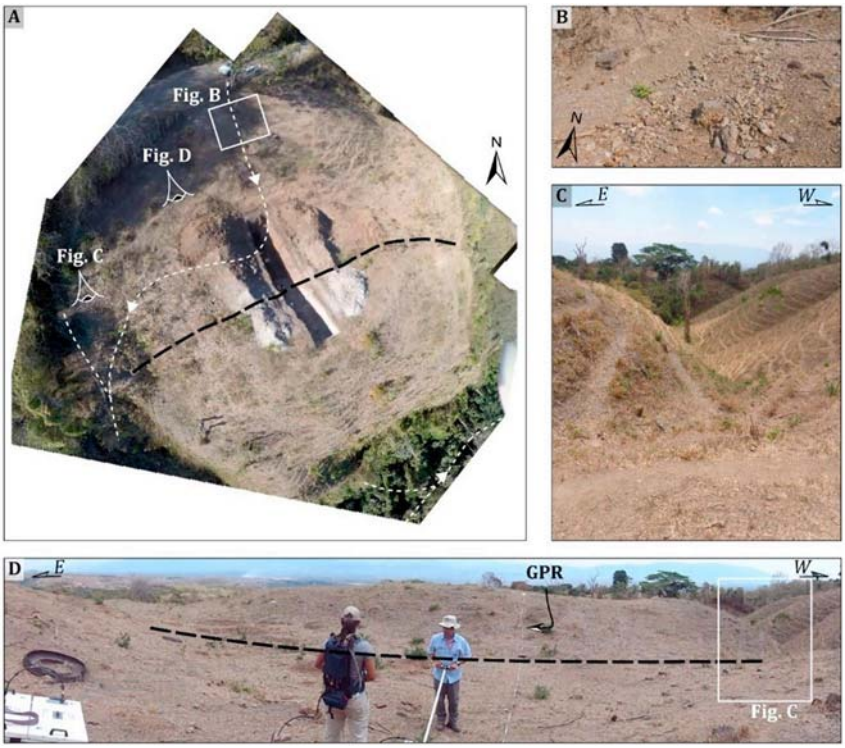

Fig. 5. Photographs of the trenching site. The dashed black lines represent the fault trace corresponding to the slope change due to the presence of the shutter ridge. The dashed white lines correspond to the principal drainages. A) The reconstituted picture of the trenching site using drone video. B) Sediments transported by drainage (arenites, decametric to centimetric angular schistose boulders). C) Offset talweg. D) Photograph taken from the north looking toward the shutter ridge located in the south.

3.2. Ground-penetrating radar acquisition

We performed ground-penetrating radar (GPR) profiles using 2D constant-offset data across the fault trace to (i) detect the fault position (in plan view and in depth) and (ii) to estimate the distribution of the faulting, with the intention of pre-sizing the trench. We used two shielded IDS antennas connected to a RIS system: a 200 MHz antenna to observe shallow units with a high resolution and an 80 MHz antenna to observe deeper units with a lower resolution. We performed two transects perpendicular to the fault trace, and for each section, two GPR surveys were carried out using each of the two available antennas.

We processed the GPR data using the Seismic Unix software (Cohen and Stockwell Jr., 2001). The main processes were 1) filtered using a "dewow" filter and "background removal" to remove a continuous bias in the data (Fischer et al., 1994), signal reverberation (Annan, 2009) and direct waves (Cassidy and Jol, 2009), 2) band pass filtering depending on the antenna to improve the signal-to-noise ratio, 3) automatic gain control (AGC) or time power gain amplification in order to amplify late arrivals that have been naturally attenuated due to geometrical spreading and soil attenuation. Finally, since no common midpoint (CMP) surveys were carried out with the shielded antennas, we had to assume a constant GPR velocity of 10 cm/ns, a standard value in this type of unsaturated formations. This velocity value was used to perform time to depth conversions and topography corrections. Due to the weak lateral reflectivity variations and the absence of diffraction hyperbolas in the images no migration was applied to the data.

3.3. Trenching and dating method

The Higuerón trench was excavated perpendicular to the fault trace. We obtained a high resolution image of the trench, with several photographs taken in different luminosity conditions. We used the Photoscan software to construct 3D images (PhotoScan).

We sampled charcoals in the horizons surrounding the ruptures to date the seismic events (Table 1). Charcoals were dated in the Laboratoire de Mesure du Carbone 14 at the CEA in Saclay (Gif-sur-Yvette, France) using a mass spectrometer (AMS) called ARTEMIS. The ages were calibrated using OxCal 4.2.3 (Lienkaemper and Ramsey, 2009; Bronk-Ramsey and Lee, 2013) and calibration curve INTCAL13 (Reimer, 2013).

4. Results

4.1. Results of the shallow geophysical survey

Two GPR acquisitions were carried out (80 MHz and 200 MHz antennas) along two profiles perpendicular to the fault trace (L0 and L1, see localization in Fig. 5-d and Fig. 6-a). We observe lateral discontinuities of some reflectors on these four GPR profiles, located below the main break of the topography slope (Fig. 6-b). These discontinuities are dipping (mostly northward) and recurrent, and are not due to the presence of noise in these areas. The two compartments separated by the discontinuities also show a large and abrupt change in the wave penetration, probably due to lithological variations marked by conductivity changes. Therefore these discontinuities are probably due to ruptures which bring together two different stratigraphic units. These ruptures are distributed in a 5 m strip, which allows us to pre-size a 15 m long excavation.

4.2. Trench description

The trench was excavated nearly perpendicular to the fault trace oriented N75°. The trench is oriented N170°, it is 14 m long, 1.5 m wide and up to 2.5 m deep. In the following, "MM" will be used as an abbreviation for Meter Mark, and represents the unit on the 1 m × 1 m reference grid fixed on the trench walls to make it possible to study and draw them as precisely as possible. Overall, the stratigraphy consists of two sets (whitish and brownish) comprising series of individualized units. These two layered sets are separated by the main active deformation zone (MM7-MM8) located where the topographic slope change occurs (Fig. 7 and Fig. 8). The different layers are thick (> 50 cm), clastic and homogeneous. Nineteen units have been identified, and labeled from "a" to "s" (where "a" is the youngest unit).

In the northern part of the trench (MM0-MM7), the units are deep

Table 1
Mass spectrometry measurements made at the Laboratoire de Mesure du Carbone 14 at CEA Saclay. The charcoal ages were calibrated using OxCal 4.2.4 (Bronk-Ramsey and Lee, 2013) and calibration curve INTCAL13 (Reimer, 2013). Samples marked with an * are out of stratigraphic order, and were probably reworked (cf. supplementary material Text S1). BCE-CE = Before Commun Era-Commun Era. Radiocarbon dating on soils is more complex. However, it is possible that this average age (AMRT age) takes inherited or remobilized components into account. Several methods exist to calibrate these AMRT ages: 1) no calibration since the age is an average (Schaetzl and Anderson, 2005), and 2) calibration with a curve and by doubling the uncertainties measured by the laboratory (Nelson et al., 2006; DuRoss et al., 2008). For this study, we will not calibrate the ages. For surface soil, it is quite common for the AMRT age to be older than an age obtained from charcoal sampled in the soil (e.g., Nelson et al., 2006). Several authors have subtracted an inferred mean residence time from the AMRT age (MRT correction). This MRT correction is based on an inferred age of the soil when it was at the surface. To obtain this MRT, they compare the AMRT age of the soil at the surface and an AMS age of the charcoal sampled within the soil (e.g., Nelson et al., 2006; DuRoss et al., 2008; DuRoss et al., 2014). Unfortunately, this method cannot be applied here, since the difference between the ages of the charcoal and soil is 3000 years in average, which implies that the uncertainty is too high (e.g., in unit "a", Hi-CE18 yields an age of 85 ± 30 BP, whereas Hi-SE6 gives an age of 3000 ± 30 BP). Therefore, we will use a soil age assuming it reflects a weighted mean of the ages of the various organic components.

Samples	*Type*	*Mg C*	*Delta C13*	*pMc*	*Error pMC*	*Age B.P.*	*Error Age B.P.*	*Age Calibrated (2-σ) in BCE-CE.*	*Units*
HI-CE2	Charcoal	0.27	-21.9	75.05	0.63	2310	70	*	a
HI-CE4	Charcoal	1.45	-23.5	81.31	0.31	1660	30	*	b
HI-CE5	Charcoal	1.47	-24.6	89.20	0.27	920	30	*	a
Hi-CE6	Charcoal	0.86	-29.6	97.84	0.31	175	30	1656 - …	a
HI-CE9	Charcoal	1.81	-22.9	88.42	0.26	990	30	*	b
HI-CE10	Charcoal	1.62	-25.0	89.20	0.28	920	30	*	e
HI-CE13	Charcoal	1.09	-26.2	88.74	0.28	960	30	*	e
HI-CE17	Charcoal	0.68	-26.9	98.73	0.31	105	30	1681-1937	c
Hi-CE-18	Charcoal	1.38	-26.4	98.96	0.30	85	30	1688-1927	a
HI-CE21	Charcoal	0.78	-23.6	99.11	0.32	70	30	1691-1924	a
HI-CE22	Charcoal	1.48	-23.3	33.86	0.19	8700	45	*	e
Hi-CE23	Charcoal	1.78	-25.9	79.48	0.27	1845	30	*	e
HI-CE24	Charcoal	Failed to prepare							e
HI-CE27	Charcoal	1.31	-25.3	29.60	0.19	9780	50	*	h
HI-CE28	Charcoal	1.52	-27.4	30.09	0.19	9650	50	*	h
HI-CO1	Charcoal	1.41	-27.7	95.68	0.28	355	30	1453-1635	h
HI-CO2	Charcoal	1.52	-24.7	98.10	0.29	155	30	1666- …	a
Hi-CO6	Charcoal	0.36	-27.0	98.12	0.33	150	30	1666- …	b
HI-CO7	Charcoal	1.44	-22.8	31.44	0.18	9295	45	-8699 - -8347	i
Hi-SE-01	Bulk	0,629	-22,93	64,95	0,25	3465	30		b
Hi-SE-02	Bulk	1,061	-20,88	77,71	0,29	2025	30		b
Hi-SE-03	Bulk	0,843	-17,43	24,31	0,18	11360	60		f
Hi-SE-04	Bulk	0.97	-19.8	43.94	0.20	6605	40		c
Hi-SE-06	Bulk	0.90	-19.7	68.79	0.25	3005	30		a
Hi-SE-07	Bulk	1,071	-19,11	50,91	0,24	5425	35		e
Hi-SE-08	Bulk	0.97	-19.4	52.28	0.23	5215	35		a
Hi-SE-09	Bulk	0,812	-15,94	32,79	0,21	8960	50		n
Hi-SE-10	Bulk	0,437	-19,11	44,57	0,26	6490	45		l
Hi-SE-11	Bulk	0,962	-19,94	43,76	0,26	6640	50		q
Hi-SE-12	Bulk	0,935	-19,94	63,84	0,28	3605	35		m
Hi-SE-21	Bulk	0,702	-14,07	14,77	0,18	15360	100		m
Hi-S0-01	Bulk	1,332	-17,71	53,79	0,32	4980	50		p
AMS-E1	Bulk	1,36	-22,0	71,77	0,25	5040	35		a
AMS-E2	Bulk	0,17	-22,1	39,40	0,28	2665	30		d
AMS-O1	Bulk	0,79	-22,8	77,07	0,25	7480	60		m/a
AMS-O2	Bulk	1,36	-22,0	71,77	0,25	2095	30		a

brown and constituted of centimetric to decimetric angular schist clasts. The basal units are mostly characterized by a compact clayed matrix. In the upper sequence, the matrix is less compact. The quarzitic basement (unit "s") appears at the northernmost extremity of the trench (MM1-MM2), and is wrapped by an orangey brown compact layer composed of decimetric angular schist clasts in a clayey matrix.

In the southern part below the shutter ridge (MM7-MM13), the whitish layers are carbonated, friable and composed of angular schist blocks. These blocks are larger ($> 40\ cm^3$) toward the upper units. The bedrock (unit "r") appears in the trench bottom and consists of a foliated, friable and weathered rock with a patina ocher grey. Between MM8 and MM9 the bedrock appears crushed.

Two zones of active brittle deformation can be identified in the trench, annotated ZONE-1 and ZONE-2. ZONE-1 is located between MM1 and MM5, the deformation is accommodated by vertical faults (F1 to F5 and F22 to F25), dipping faults (F6 and F7) and by one open crack (between F2 and F3). The second zone of faulting is the main deformation zone, which is located between MM6 and MM9 in the eastern wall and between MM7 and MM8 in the western wall. It is the zone separating the two sedimentary sets, coinciding with both the slope change in the topography and where the deformation is identified in the GPR profiles (Fig. 6 and Fig. 8). The deformation is accommodated by vertical or north highly dipping faults (F8 to F16 and F17 to F19).

The charcoals were primarily sampled in units "a", "b", "c", "e" and "h" (Table 1) and radiocarbon dating was performed following the method given in Section 3.3; some charcoals are out of stratigraphic order, and have probably been reworked (see supplementary material Text S1). It was more difficult to interpret the radiocarbon dating

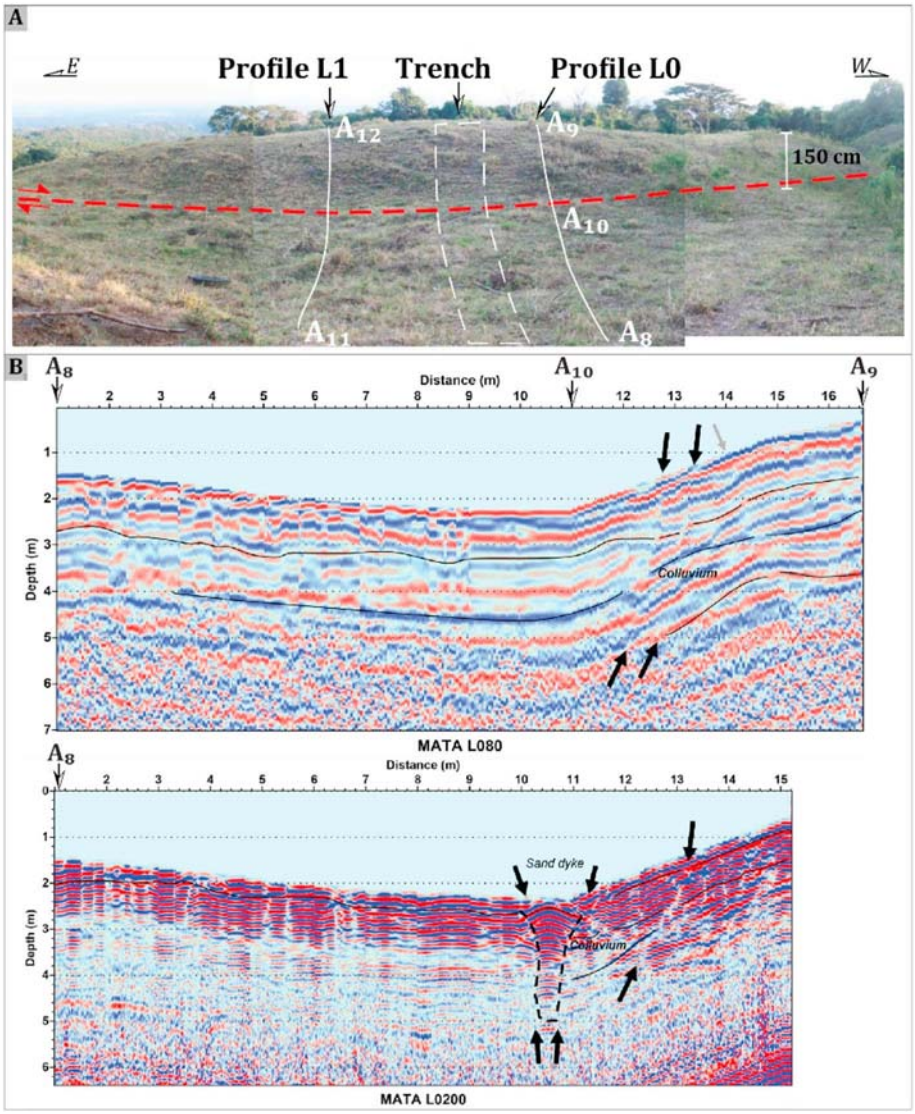

Fig. 6. A) L0 and L1 GPR profiles and relative location to the trench. The main fault trace appears as a dashed red line. B) L0 profile (oriented N175°) carried out with the 80 MHz and 200 MHz antennas, respectively, MATA L080 profile and MATA L0200 profile. The MATA L080 profile shows the first 4–5 m in depth. At higher resolution, the MATA L0200 profiles shows the first meter in depth. The black arrows indicate discontinuities. (L1 profiles are shown in Fig. S3). (For interpretation of the references to color in this figure legend, the reader is referred to the web version of this article.)

results on soils as soil is composed of several organic components at various ages and at different states of decomposition. Dates given by the radiocarbon measure are called AMRT ages (Average Mean Residence Time) and reflect a weighted mean of the ages of the various organic components (Machette et al., 1992; Schaetzl and Anderson, 2005). It is quite common that the AMRT age for surface soil is older than an age obtained from charcoal sampled within the soil (e.g., Nelson et al., 2006). In this trench, the difference between the ages of the charcoal and the soil is 3000 years in average (e.g., in unit "a", Hi-CE18 yields an age of 85 ± 30 BP, whereas Hi-SE6 gives an age of 3000 ± 30 BP). Given that this difference is difficult to explain and to correct, we will consequently not use soil ages.

4.3. Description of the units and seismic events

The units were deposited within different conditions (see the stratigraphic column in Fig. 7). Units "h", "p" and "q" are alluvial in origin since they comprise rounded to regular aligned (or semi-sorted) gravels. Units "e", "i", and "j", were deposited in a pond environment since they are constituted of fine and organic sediment and are localized in a topographic depression. Units "b", "c", "f", "k", "l", "m", "n", and "o" are gravitational deposits filling open cracks, likely created by seismic events. Units "e" and "g" are interbedded: "g" is a sheet flood or a debris flow deposit due to its high amount of decimetric schists and oriented blocks and "e" is probably a pond deposit. Finally, unit "d" is probably a gravitational deposit such as a colluvial wedge.

The identification of seismic events is based on upward terminations of cracks and on open cracks (e.g., Fumal et al., 2002; Audemard, 2005). Three main events have been identified (called E1, E2 and E3), and given that these events ruptured the ground, the magnitude of these events is probably at least M_w 6–6.5 (McCalpin, 2009). Fig. 9 shows the proposed chronological succession of events E1, E2 and E3.

- Event E1

E1 refers to various successive events characterized by ruptures and open cracks located in ZONE-2 with no chronological relationships among them, but which are all sealed by the same sedimentary unit. In this zone, there are six deformation features within the eastern wall (from F9 to F14) and two within the western wall (F17?-F20-F21). They

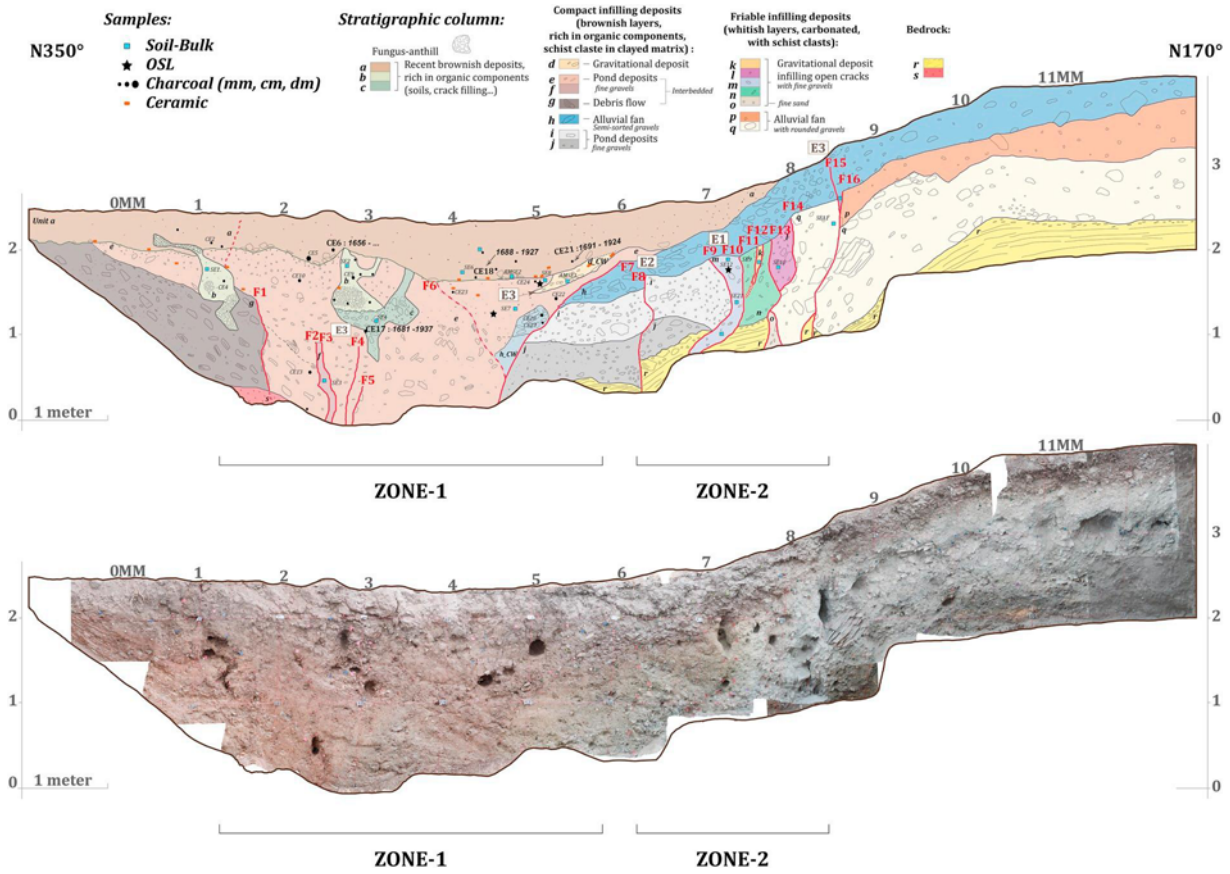

Fig. 7. Eastern wall of the Higuerón trench (log and photographic mosaic). ZONE-1 and ZONE-2 correspond to the main zone of active deformation, the faults are denoted from F1 to F16 and the deduced events are denoted from E1 to E3. MM corresponds to Meter Mark and is used to find one's bearings in the referenced grid along the trench walls. At the bottom, GPR profile MATA L0200 carried out with a 200 MHz antenna.

are sealed by unit "h", dated at 1456–1636 CE (charcoal Hi-C01). Event E1 is therefore older than this age. The event is post 8699–8347 BCE (Hi-CO7 in unit "I"). Unfortunately, we cannot use the samples taken from inside the cracks (i.e. Hi-SE12 dated at 3605 ± 35 BP) since the dating results for the soil in this trench were not satisfactory probably due to reworking.

- Event E2

This event is characterized by ruptures F7, F8 (eastern wall) and F22 (equivalent to F7 but in the western wall). This event affected unit "h". In the eastern wall, a colluvial wedge was deposited and preserved (unit "h_CW"). Ruptures are sealed by unit "e" which is not dated but unit "e" is faulted by event E3, and therefore E2 is older than E3 (Fig. 9-step Sedimentation). The age model carried out with OxCal, which considers E2 as younger than the charcoal Hi-C01 from unit "h" and E2 as older than E3 (see below), indicates that the event occurred between 1483 and 1743 CE (Fig. 10).

- Event E3

This event is characterized by ruptures F15, F16, F1 to F6 (eastern wall), F18, F19, F23, F24 and F25 (western wall). Faults F15 (eastern wall), F18 and F19 (western wall) created a decimetric scarp that is still visible at the surface. Unit "d_CW", which is only recognized in the eastern wall, is interpreted as the preserved colluvial wedge associated with the scarp, which was then partially eroded and recovered by unit "a" (Fig. 9-step Erosion and Sedimentation). Faults F15 and F18 affect unit "h", which was dated between 1456 and 1636 CE (Hi-CO1). E3 is older than unit "a", which is not affected by cracks. This unit is dated by four samples (Hi-C02, Hi-CE06, Hi-CE21 and Hi-CE18). An OxCal age model has been calculated assuming that the four samples have not been deposited in a stratigraphic order but in "phase"; in this case, E3 occurred between 1545 and 1825 CE (2-sigma) (Fig. 10).

This estimation can be more accurate if the areas located in MM3 (eastern wall) and MM2 (western wall) are considered as open cracks related to E3 (and today partially colonized by fungus-anthill). Under this assumption, E3 also corresponds to ruptures F4, F5 (and probably F1, F2 and F3) in the eastern wall and to ruptures F25 and F23 in the western wall. Two charcoals (Hi-CO6, Hi-CE17) were collected (apart from the area colonized by ants) in a material made of centimetric clasts that should come from the filling of the crack due to the removal of soil at the surface. Charcoals should therefore be older than event E3, in this case the OxCal model indicates that E3 occurred between 1696 and 1876 CE (Fig. S5 in the supplementary material).

- Two or three events?

It could be argued that events E2 and E3 are in fact the same event since the faults attributed to E2 are attenuated strands in units "h" and "e". The Oxcal model gives a date of 1502–1782 CE (2 sigma) for this event (see Fig. S10 in the supplementary material). In this case, unit "e" was deposited before the event and, in order to achieve the observed configuration, the cinematic of the fault F22 and F7 should be mainly dextral and unit "e" should be deposited in a channel environment (see Fig. S9 in the supplementary material). In this case, unit "e" should therefore be faulted by F7 however this is not observed. In fact, F7 is sealed by unit "e". We also observe two colluvial wedges in the eastern wall: unit "d_CW" associated with event E3 and "h_CW" due to event E2 and sealed by unit "e" (Fig. 9). Based on this, we suggest that two events occurred.

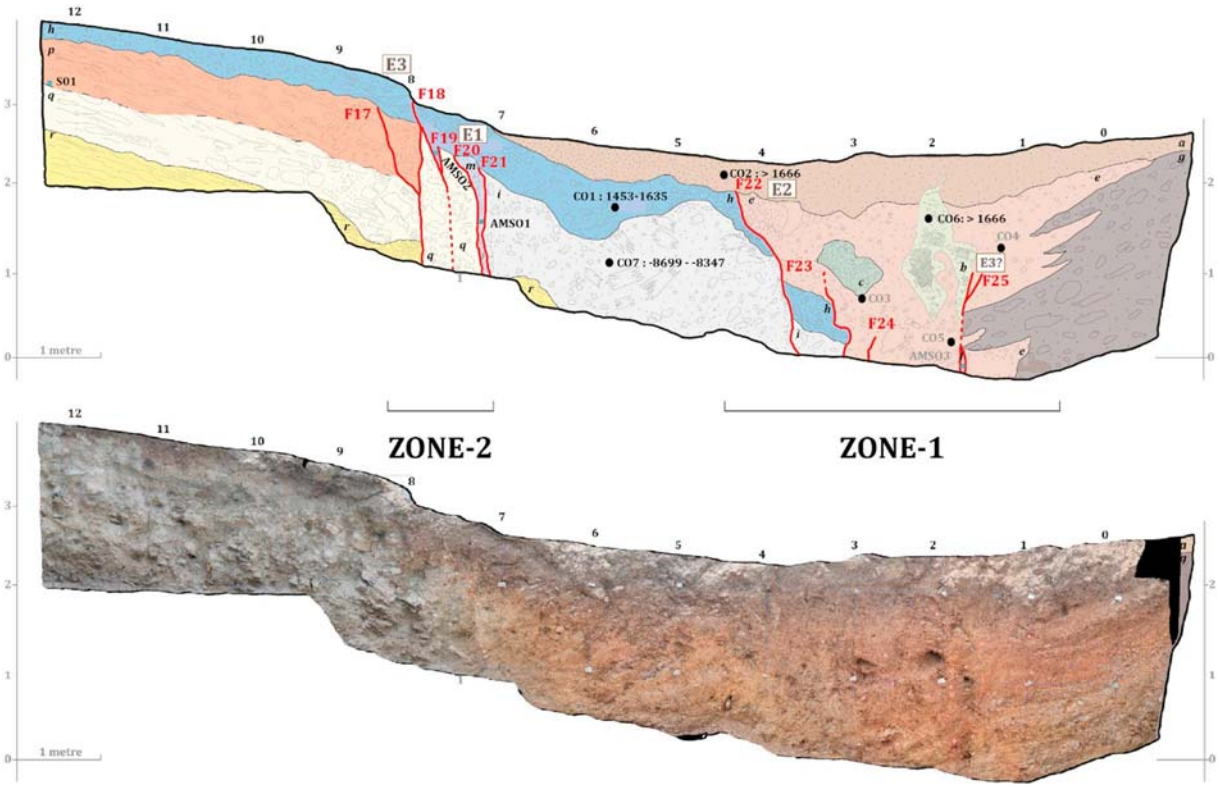

Fig. 8. Log of the western wall, GPR profile MATA L080 carried out with an 80 MHz antenna and photogrammetry mosaic. The ZONE-2 ruptures were imaged by the GPR profile.

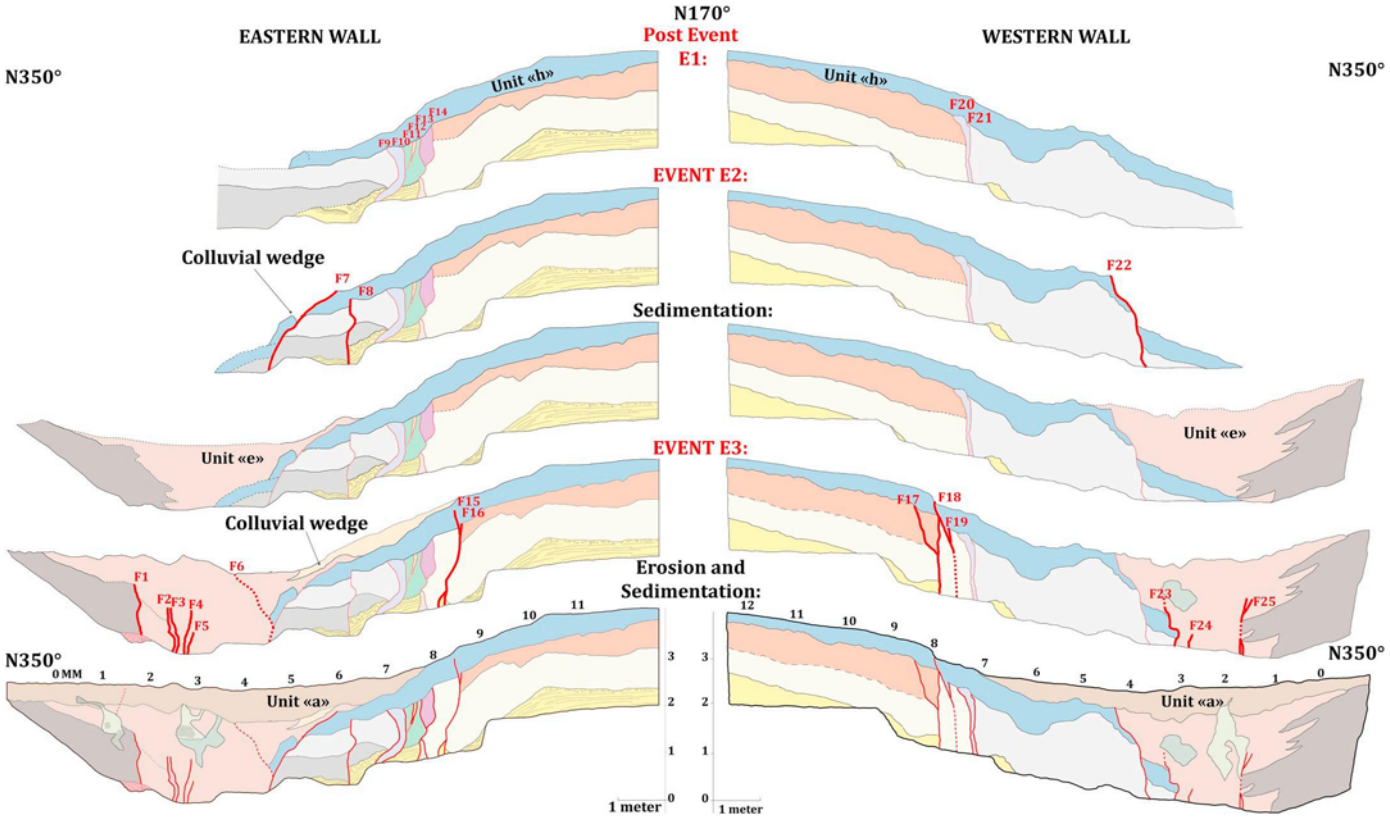

Fig. 9. Reconstructions of the events that occurred in the Higuerón trench.

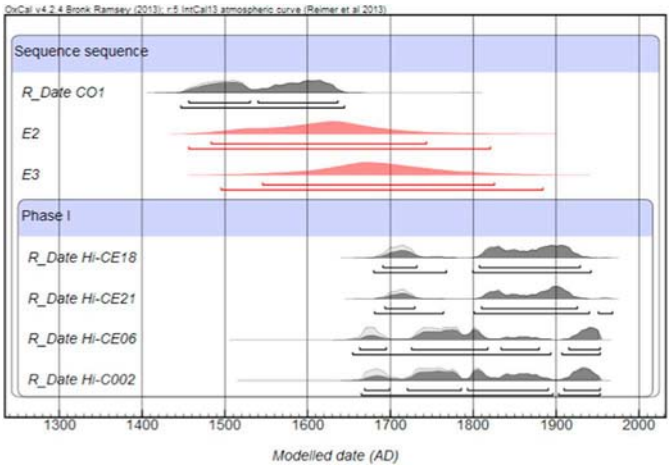

Fig. 10. Age model calculated for events E2 and E3 using OxCal v4.2.4 (Bronk-Ramsey and Lee, 2013) and calibration curve IntCal13 (Reimer, 2013). The light grey distributions indicate raw calibrations whereas dark grey distributions indicate modelled ages. "Phase" sets are sets of samples where no stratigraphic order is assumed. The age model indicates that younger ages could be more recent.

5. Discussion

5.1. Capability and limits of ground-penetrating radar in this study

Here in this context, the GPR analysis reveals the main fault zone which corresponds to the main lithological variation: clayed matrix layers in contact with carbonated layers. On the one hand, in the clayed units, the electromagnetic waves penetrate at shallower depths regardless of the antenna frequency. This observation is consistent with an increase in electrical conductivity in clays. On the other hand, the main lithological variations are better observed in profiles derived using the 80 MHz antenna (Fig. 6 and Fig. 8). Secondary or deeper strands were not revealed in the GPR profiles, nor were the different units that were identified in the nearby trench; this probably due to the clay content and the lack of resolution. The different units are probably characterized by similar electromagnetic proprieties, this avoid to resolve unit geometry. However the GPR results also suggest that the fault zone is active and that it was worthwhile to dig a trench at this site (e.g., Ercoli et al., 2013; Grützner et al., 2016).

5.2. Link with historical seismicity and return period

For event E3, following the various assumptions made above, the dates calculated by the OxCal age model vary between 1545 and 1825 CE or between 1696 and 1876 CE (Fig. 10 and Fig. S5 in the supplementary material). This means that this event may correspond to both the 1736 and 1812 CE historical earthquakes. However, with regard to the magnitude of 7.4 inferred from the archives (Choy et al., 2010), the 1812 event had a maximum intensity within this area, and it is likely that here 1) the fault broke reaching the surface; and 2) strong shaking collapsed most of the previous tectonic scarps into loose material. In particular, the damages related to the 1812 earthquake located near the fault are numerous, well documented, and consistent with a magnitude Mw > 6, which is not the case for the 1736 event whose magnitude does not seem to be as large as Mw 7 based on the evaluation of the historical documents (see Martinez Silva et al., 2016). Since the 1812 event is the last one that ruptured this fault segment, a slip deficit of 1.7–2.3 m can be estimated using a preferred Quaternary slip rate of 8.4–11.2 $mm{\cdot}a^{-1}$ (Pousse-Beltran et al., 2017). This slip deficit corresponds to a Mw ~7 event according to Leonard's (2010) scaling relation.

The Higuerón trench analysis enables to recognize two other events not identified by Audemard (2016) in his two paleoseismological studies: E1 and E2. Event E1 is estimated to occur before 1456–1636 CE and after 8699–8347 BCE. Event E2 occurred between 1483 and 1743 CE. (2 sigma). As a result, the 1736 earthquake may correspond to event E2 because although poorly documented, the archives mention damage (intensity VII) in the cities of Barquisimeto and Guama located near the fault segment studied here (Grases et al., 1999; Martinez Silva et al., 2016). Based upon this hypothesis, the slip accumulated from 1736 until the 1812 event was 0.6–0.8 m; this slip deficit does not correspond to a Mw 7.4 event (according to Wells and Coppersmith's relation). Therefore, it is possible that: (1) not all of the strain was released during the 1736 event or (2) the Boconó Fault follows a clustered earthquake behavior (e.g., Ben-Zion et al., 1999; DiCaprio et al., 2008; Benedetti et al., 2013; Klinger et al., 2015). Other Boconó segments seem to show this behavior (Fig. 11). For example, the Manzanos and Primavera trenches excavated along the adjacent Boc-d segment (Audemard, 2014) can be used to identify several events that occurred in a short timespan (every 140 to 600 years).

In the case of E2 not being the 1736 event, event E2 takes place between 359 and 76 years before 1812 CE. Thus, in any case, the studied segment fault (Boc-e) is able to trigger $M_w \geq 6$–6.5 events every few centuries. Before Common Era, the Quigua trench study (located 3–4 km away from the trench studied here) established a return period of 2500 to 3000 years in average. Two assumptions can be proposed to explain this paradox: (1) the behavior of the fault changed since 1500 CE and thereupon the fault entered into a period of intense earthquake activity and/or (2) a part of the Holocene deformation is missing in the Quigua trench. The second assumption seems much more

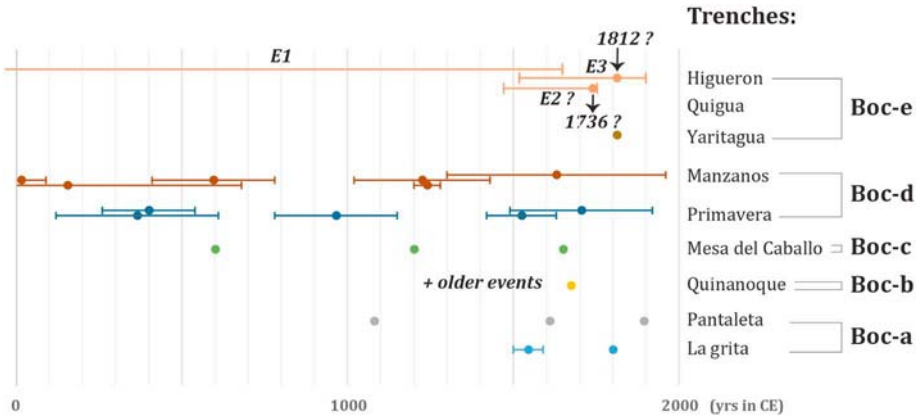

Fig. 11. Identified events in CE in trenches excavated along the Boconó Fault (Beltran et al., 1990; Audemard, 1997, 1998, 2014, 2016; Audemard et al., 1999, 2008; Alvarado et al., 2008). Events without error bars are events where the uncertainties are poorly detailed in the studies.

likely as the preferred Quaternary slip rate estimated by Pousse-Beltran et al. (2017) of 8.4–11.2 mm·a^{-1} is consistent with geodetic data (~12 mm·a^{-1}) (Pérez et al., 2011; Reinoza, 2014; Symithe et al., 2015).

In the case where events E2 and E3 are the same event (see discussion "Two or three events?"), the Oxcal age model ranges from 1502 and 1782 (2 sigma). The 1812 event is a candidate for the surface break considering uncertainties of 3 sigma (1464–1854 CE), however the 1736 event could be also a candidate for this. Since the magnitude of the 1736 event cannot be evaluated due to the scarcity of data on the damages (i.e. a totally ruined church in Guama and a severely damaged one in Barquisimeto (Silva et al., 2016)), it is difficult to discriminate between the two events. However, as we described earlier in this contribution, several studies have pointed out that the 1812 event had a magnitude Mw > 7, the rupture reached the surface and the intensity center was located nearby the trench (Fig. 2-b). The 1812 event was also inferred to be responsible for the surface break in the Yaritagua trench (Audemard, 2016). If this is the case, based on the distance between both trenches, the 1812 event triggered by the Boconó Fault ruptured the ground surface over a distance of at least ~30 km.

6. Conclusion

Detailed studies on the Higuerón trench site allow us to identify three events: an event E1 that took place after 8699–8347 BCE and prior to 1456–1636 CE, a second event E2 that occurred between 1483 and 1743 CE and finally a last event E3 that occurred between 1545 and 1825 CE. Unfortunately, our morphotectonic results in Higuerón did not allow to shedding light on prehistorical history but provides a new view in the historical seismicity, although recent (XVIII–XIV centuries) and still poorly known in Venezuela. Furthermore, based on the historical archives and previous trench studies, we can attribute an age of 1812 CE for the third seismic event (E3), similar to the age inferred at the Yaritagua trench site (Audemard, 2016).Hence, the 1812 CE seismic event may have produced a 30 km long surface rupture zone. Moreover, if the 1812 event had released all of the accumulated strain, a slip deficit of 1.7–2.3 m can be estimated using a preferred Quaternary slip rate of 8.4–11.2 mm·a^{-1} (Pousse-Beltran et al., 2017). This slip deficit corresponds to the Mw ~7 event. To consolidate our "slip deficit" model, a 3D trenching survey will be necessary. This method will be used to reconstruct the slip per event. This technique will also give a relevant magnitude value to be compared with the 1812 magnitude value estimated using the intensity data. Concerning event E2, our interpretation of the present trench supports two distinct events, E1 and E2, although this interpretation could possibly be disputed in the light of new trenches or undiscovered archives. Currently, from our point of view event E2 might correspond to the 1736 event, although this is poorly documented. If not, two events occurred within a time span of 359 to 76 years. Therefore, future seismic hazard assessments should consider that the northernmost segment of the Boconó Fault (Boc-e) is able to trigger Mw 6+ events every few hundred years.

Acknowledgments

This work is part of the PhD thesis written by L. Pousse Beltran (ISTerre, USMB) and funded by the French Ministry of Higher Education and Research. We are especially grateful to L. Audin for offering us radiocarbon dating. We thank the Bolivarian Government of the Yaracuy State of Venezuela (contact: Lic. Dany Bozán), the townhalls of San Felipe (contact: Ing. Tony Mata) and San Pablo, Municipio Arístides Bastidas (contacts: Liv Marvit Méndez, Ing. Daniel Rivas) and the foundation "Yaracuy Bonito" (contacts: Ing. Luiz Muñoz, Ing. Renny Aldeño) for providing us with backhoes, and the landlords Mr. Roberto Sánchez, Mr. Idelfonso Rojas and Mr. Marcial García Roque for allowing us to dig on their land. We would also like to thank Bartolo and William for driving the backhoes. We thank Y. Klinger, J.-F. Ritz, A. Singer, and L. Rodriguez for their advice and fruitful discussions. We also thank Grace Bato for suggestions regarding the English content. Xavi Gallach and the Edytem laboratory are thanked for carrying out the photogrammetry processes and P. Lacroix is thanked for help with the DEM processing. The authors thank the Fundacion Venezolana de Investigaciones Sismologicas (FUNVISIS) for the aerial photographs, topographic maps, archives of the Venezuela study area, and the logistical support given during the fieldwork. We thank SMA Artemis of the LMC14 (INSU) for the radiocarbon dating and subventions and Mr. Dumoulin for processing the radiocarbon dating data. We acknowledge GIAME, FONACIT and ECOS (project: FONACIT-ECOS Nord PI 2009000818, FONACIT 2012002202 and 2013000361) for financial support during the field trip. This investigation was also funded by ISTerre-Sud, IRD, ISTerre BQR, and USBM (AAP). This work has been also supported by a grant from Labex OSUG@2020 (Investissements d'avenir – ANR10 LABX56). The Pleiades images were obtained through an ISIS project funded by the CNES, the French Space Agency.

Appendix A. Supplementary data

Supplementary data to this article can be found online at https://doi.org/10.1016/j.tecto.2018.09.010.

References

Altez, Rogelio, 2005a. El terremoto de 1812 en la ciudad de Caracas: un intento de microzonificación histórica. Revista Geográfica Venezolana 46, 171–198.
Altez, Rogelio, 2005b. Todo lo que se movió en 1812 en la placa del Caribe: sismos, volcanes y transmisión de energía. Revista Geográfica Venezolana 143–170.
Altez, Rogelio, 2006. El Desastre de 1812 en Venezuela: Sismos, Vulnerabilidades Y Una Patria no Tan Boba. Universidad Catolica Andres.
Altez, Rogelio, 2016. The earthquakes of the March 26th 1812 in Venezuela: new contributions and evidences on these effects. Revista de La Facultad de Ingeniería 31 (1).
Alvarado, M., Audemard, Franck, Laffaille, Jaime, Ollarves, R., Rodríguez, Luz M., 2008. Paleoseismic investigation on the Boconó Fault, between Las González and Estanques, Mérida Andes, Venezuela. In: 7th International Symposium on Andean Geodynamics (ISAG 2008, Nice), Extended Abstracts, pp. 37–40.
Annan, A.P., 2009. Electromagnetic Principles of Ground Penetrating Radar. Vol. 1 Elsevier Science Ltd, Oxford.
Audemard, Franck, 1997. Holocene and historical earthquakes on the Boconó fault system, Southern Venezuelan Andes: trench confirmation. J. Geodyn. 24 (1–4), 155–167. https://doi.org/10.1016/S0264-3707(96)00037-3.
Audemard, Franck, 1998. Contribución de la paleosismología a la sismicidad histórica: los terremotos de 1610 y de 1894 en los Andes Venezolanos Meridionales. Revista Geográfica Venezolana 39, 1–2.
Audemard, Franck, 2002. Ruptura de los grandes sismos historicos Venezolanos de los siglos XIX y XX revelados por la sismicidas intrumental contemporanea. In: 11° Congreso Venezolano de Géofisica, pp. 17–20 (Caracas, Venezuela).
Audemard, Franck, 2005. Paleoseismology in Venezuela: objectives, methods, applications, limitations and perspectives. In: Tectonophysics, Paleoseismology Integrated Study of the Quaternary Geological Record for Earthquake Deformation and Faulting. 408 (1–4). pp. 29–61. https://doi.org/10.1016/j.tecto.2005.05.034.
Audemard, Franck, 2008. Historia Sísmica y Segmentación Sismogenética de La Falla de Boconó Con Base En El Análisis Geológico de Sedimentos Recientes Deformados (Por Vía de Trincheras y Núcleos Continuos). (Proyecto Fonacit 2001002492).
Audemard, Frank, 2009. 5.3.8 Falla de Boconó (VE-06b y VE-06c). In: Atlas de Deformaciones Cuaternarias de Los Andes. Servicio Nacional de Geologia y Mineria, 7:259–71. Servicio Nacional de Geologia y Mineria. Andino, Proyecto Multinacional and para las Comunidades Andinas, Geociencias.
Audemard, Franck, 2014. Segmentación sismogenética de la falla de boconó a partir de investigaciones paleosísmicas por trincheras, Venezuela occidental: ¿migración de la ruptura hacia el noreste en tiempos históricos? Rev. Asoc. Geol. Argent. 71 (2), 247–259.
Audemard, Franck, 2016. Paleoseismic assessment of the San Felipe segment of the Bocono fault (Northwestern Venezuela): response for the March 26th, 1812 earthquake? Boletin de Geología 38 (1), 125–149. https://doi.org/10.18273/revbol.v38n1-2016007.
Audemard, Felipe E., Audemard, Franck, 2002. Structure of Merida Andes, Venezuela: relations with South America-Caribbean geodynamic interaction. Tectonophysics 345, 299–327.
Audemard, Franck, Pantosti, D., Machette, M., Costa, C., Okumura, K., Cowan, H., Diederix, H., et al., 1999. Trench investigation along the Merida section of the Boconó Fault (Central Venezuelan Andes), Venezuela. Tectonophysics 308 (1–2), 1–21. https://doi.org/10.1016/S0040-1951(99)00085-2.
Audemard, Franck, M.N. Machette, J.W. Cox, R.L. Dart, and K.M. Haller. 2000. "Map and Database of Quaternary Faults in Venezuela and Its Offshore Regions - Scale 1:2 000 000." USGS Open-File Report, Open-File Report, 78 p.
Audemard, Franck, Ollarves, Reinaldo, Bechtold, Michel, Diaz, Gustavo, Beck, Christian, Carrillo, Eduardo, Pantosti, Daniela, Diederix, Hans, 2008. Trench investigation on

the main strand of the Bocono Fault in its central section, at Mesa Del Caballo, Merida Andes, Venezuela. Tectonophysics 459 (1–4), 38–53. https://doi.org/10.1016/j.tecto.2007.08.020.
Bakun, W.H., Wentworth, C.M., 1997. Estimating earthquake location and magnitude from seismic intensity data. Bull. Seismol. Soc. Am. 87 (6), 1502–1521.
Bellizzia, A., Pimentel, N., Bajo, R., 1976. Mapa Geologico Estructural de Venezuela, 1:500000, Ministerio de Minas e Hidrocarburos. Foninves, Venezuela.
Beltran, C. 1994. "Trazas Activas y Síntesis Neotectónica de Venezuela a Escala 1: 2.000. 000." In VII Congreso Venezolano de Geofísica, 541–47. Caracas, Venezuela.
Beltran, C., Giraldo, C., Singer, A., 1990. Evaluation of Recent Tectonic Activity of the Boconó Fault Near Barquisimeto (Venezuela) Based On Trench Observation. INQUA N.C., pp. 13.
Benedetti, Lucilla, Manighetti, Isabelle, Gaudemer, Yves, Finkel, Robert, Malavieille, Jacques, Pou, Khemrak, Arnold, Maurice, Aumaître, Georges, Bourlès, Didier, Keddadouche, Karim, 2013. Earthquake synchrony and clustering on Fucino Faults (Central Italy) as revealed from in situ 36Cl exposure dating. J. Geophys. Res. Solid Earth 118 (9), 4948–4974. https://doi.org/10.1002/jgrb.50299.
Ben-Zion, Yehuda, Dahmen, Karin, Lyakhovsky, Vladimir, Ertas, Deniz, Agnon, Amotz, 1999. Self-driven mode switching of earthquake activity on a fault system. Earth Planet. Sci. Lett. 172 (1–2), 11–21. https://doi.org/10.1016/S0012-821X(99)00187-9.
Bronk-Ramsey, Christopher, Lee, Sharen, 2013. Recent and planned developments of the program OxCal. Radiocarbon 55 (2–3), 720–730.
Carcaillet, Julien, Angel, Isandra, Carrillo, Eduardo, Audemard, Franck, Beck, Christian, 2013. Timing of the Last Deglaciation in the Sierra Nevada of the Mérida Andes, Venezuela. Quat. Res. 80 (3), 482–494. https://doi.org/10.1016/j.yqres.2013.08.001.
Casas-Sainz, Antonio, 1991. Estudio Sismotectonico Del Valle de Yaracuy. informe FUNVISIS, Caracas, Venezuela.
Cassidy, Nigel J., Jol, H.M., 2009. Ground penetrating radar data processing, modelling and analysis. In: Ground Penetrating Radar: Theory and Applications, pp. 141–176.
Ceballos, Angel, Angel, Isandra Fortuna, 2016. Late Pleistocene Deglaciation Histories in the Central Mérida Andes (Venezuela) (Ph. D. thesis). Université Grenoble Alpes. https://tel.archives-ouvertes.fr/tel-01310303/document.
Centeno Graü, M., 1969. Estudios sismológicos. Academia Nacional de Ciencias Físicas, Matemáticas y Naturales. In: Talleres Tipo-Litográficos de La Dirección de Cartografía Nacional, segunda edición. pp. 366 (Caracas).
Choy, José E., Palme, Christl, Guada, Carlos, Morandi, María, Klarica, Stephanie, 2010. Macroseismic interpretation of the 1812 earthquakes in Venezuela using intensity uncertainties and a priori fault-strike information. Bull. Seismol. Soc. Am. 100 (1), 241–255. https://doi.org/10.1785/0120080345.
Cluff, Lloyd S., Hansen, William R., 1969. Seismicity and Seismic-Geology of Northwestern Venezuela. Woodward-Clyde Associates.
Cohen, J.K., Stockwell Jr., J.W., 2001. CWP/SU: Seismic Unix Release 35: A Free Package for Seismic Research and Processing. Center for Wave Phenomena, Colorado School of Mines.
Colletta, Bernard, Roure, François, de Toni, Bruno, Loureiro, Daniel, Passalacqua, Herminio, Gou, Yves, 1997. Tectonic inheritance, crustal architecture, and contrasting structural styles in the Venezuela Andes. Tectonics 16 (5), 777–794. https://doi.org/10.1029/97TC01659.
Colón, Sirel, Audemard, Franck, Beck, Christian, Avila, J., Padrón, C., De Batist, M., Paolini, M., Leal, A.F., Van Welden, A., 2015. The 1900 Mw 7.6 earthquake offshore north–central Venezuela: is La Tortuga or San Sebastián the source fault? Mar. Pet. Geol. 67, 498–511. https://doi.org/10.1016/j.marpetgeo.2015.06.005.
DeMets, Charles, Gordon, Richard G., Argus, Donald F., 2010. Geologically current plate motions. Geophys. J. Int. 181 (1), 1–80. https://doi.org/10.1111/j.1365-246X.2009.04491.x.
Dhont, Damien, Monod, Bernard, Hervouët, Yves, Backé, Guillaume, Klarica, Stéphanie, Choy, José E., 2012. 3D geological modeling of the Trujillo block: insights for crustal escape models of the Venezuelan Andes. J. S. Am. Earth Sci. 39 (November), 245–251. https://doi.org/10.1016/j.jsames.2012.04.003. (Tectonic and Climatic Shaping of the Northern Andes and Southern Caribbean Margin).
DiCaprio, Christopher J., Simons, Mark, Kenner, Shelley J., Williams, Charles A., 2008. Post-seismic reloading and temporal clustering on a single fault. Geophys. J. Int. 172 (2), 581–592. https://doi.org/10.1111/j.1365-246X.2007.03622.x.
DuRoss, Christopher B., McDonald, Greg N., Lund, William R., 2008. Paleoseismology of Utah, Volume 17: Paleoseismic Investigation of the Northern Strand of the Nephi Segment of the Wasatch Fault Zone at Santaquin, Utah. Vol. 124 Utah Geological Survey.
DuRoss, Christopher B., Hylland, Michael D., McDonald, Greg N., Crone, Anthony J., Personius, Stephen F., Gold, Ryan D., Mahan, Shannon A., 2014. Holocene and latest pleistocene paleoseismology of the Salt Lake City segment of the Wasatch fault zone, Utah, at the Penrose drive trench site. In: Evaluating Surface Faulting Chronologies of Graben-Bounding Faults in Salt Lake Valley. New Paleoseismic Data from the Salt Lake City Segment of the Wasatch Fault Zone and the West Valley Fault Zone, Utah, pp. 1–35.
Egbue, Obi, Kellogg, James N., 2010. Pleistocene to present north Andean 'Escape'. Tectonophysics 489 (1), 248–257. https://doi.org/10.1016/j.tecto.2010.04.021.
Ercoli, Maurizio, Pauselli, Cristina, Frigeri, Alessandro, Forte, Emanuele, Federico, Costanzo, 2013. 'Geophysical Paleoseismology' through high resolution GPR data: a case of shallow faulting imaging in Central Italy. J. Appl. Geophys. 90, 27–40. https://doi.org/10.1016/j.jappgeo.2012.12.001.
Ferrer, C., 1991. Características Geomorfológicas y Neotectónicas de Un Segmento de La Falla de Boconó Entre La Ciudad de Mérida y La Laguna de Mucubají, Estado Mérida. Guía de La Excursión. Esc. Latinoamericana de Geofísica.
Fiedler, Günther, 1961. Áreas afectadas por terremotos en Venezuela. In: Memoria Del III Congreso Geológico Venezolano. 3. pp. 1791–1810.
Fiedler, Günther, 1972. La liberación de energía sísmica en Venezuela, volúmenes sísmicos y mapa de isosistas. In: Memorias Del IV Congreso Geológico Venezolano. 4. pp. 2441–2462.
Fischer, Steven C., Stewart, Robert R., Jol, Harry M., 1994. Processing ground penetrating radar data. In: Fifth International Conferention on Ground Penetrating Radar.
Freymueller, Jeffrey T., Kellogg, James N., Vega, Victor, 1993. Plate motions in the North Andean region. J. Geophys. Res. Solid Earth 98 (B12), 21853–21863. https://doi.org/10.1029/93JB00520.
Fumal, T.E., Weldon, R.J., Biasi, G.P., Dawson, T.E., Seitz, G.G., Frost, W.T., Schwartz, D.P., 2002. Evidence for large earthquakes on the San Andreas fault at the Wrightwood, California, paleoseismic site: A.D. 500 to present. Bull. Seismol. Soc. Am. 92 (7), 2726–2760. https://doi.org/10.1785/0120000608.
Giegengack, R., Grauch, R.I., Shagam, R., 1976. Geometry of Late Cenozoic displacement along the Bocono Fault, Venezuelan Andes. Boletín de Geología Publicación Especial 7 (2), 1201–1223.
Giraldo, C., 1985. Neotectonique et Sismotectonique de La Region d'El Tocuyo San Felipe (Venezuela Centro Occidental) (Ph.D. thesis). Université des sciences et techniques du Languedoc.
Grases, José, Altez, Rogelio, Lugo, Miguel, 1999. Catálogo de Sismos Sentidos o Destructores: Venezuela, 1530–1998. Vol. 37 Editorial Innovacio Niversidad Central D.
Grützner, Christoph, Fischer, Peter, Reicherter, Klaus, 2016. Holocene surface ruptures of the Rurrand Fault, Germany—insights from palaeoseismology, remote sensing and shallow geophysics. Geophys. J. Int. 204 (3), 1662–1677. https://doi.org/10.1093/gji/ggv558.
Hackley, P.C., Urbani, F., Karlsen, A.W., Garrity, C.P., 2005. Geologic Shaded Relief Map of Venezuela, US Geological Survey Open File Report, 1038. (1038. US Geological Survey Open File Report).
International Seismological Centre, 2013. On-Line Bulletin. Int. Seis. Cent, Thatcham, United Kingdom.
Kalm, Volli, Mahaney, William C., 2011. Chapter 59 - Late Quaternary glaciations in the Venezuelan (Mérida) Andes. In: Ehlers, Jürgen, Gibbard, Philip L., Hughes, Philip D. (Eds.), Developments in Quaternary Sciences. Quaternary Glaciations - Extent and Chronology 15. Elsevier, pp. 835–841. https://doi.org/10.1016/B978-0-444-53447-7.00059-3.
Kellogg, James N., Vega, Victor, Stailings, T.C., Aiken, Carlos L.V., 1995. Tectonic development of Panama, Costa Rica, and the Colombian Andes: constraints from global positioning system geodetic studies and gravity. Geol. Soc. Am. Spec. Pap. 295 (January), 75–90. https://doi.org/10.1130/SPE295-p75.
Klinger, Y., Le Béon, M., Al-Qaryouti, M., 2015. 5000 yr of paleoseismicity along the Southern Dead Sea fault. Geophys. J. Int. 202 (1), 313–327. https://doi.org/10.1093/gji/ggv134.
Laffaille, Jaime, Ferrer, Carlos, 2003. El terremoto del jueves santo en mérida: año 1812. Revista Geogràfica Venezolana 44 (1), 107–123.
Leonard, Mark, 2010. Earthquake fault scaling: self-consistent relating of rupture length, width, average displacement, and moment release. Bull. Seismol. Soc. Am. 100 (5A), 1971–1988. https://doi.org/10.1785/0120090189.
Lienkaemper, James J., Ramsey, C.B., 2009. OxCal: versatile tool for developing paleoearthquake chronologies—a Primer. Seismol. Res. Lett. 80 (3), 431–434. https://doi.org/10.1785/gssrl.80.3.431.
Machette, M.N., Personius, S.F., Nelson, A.R., 1992. Paleoseismology of the Wasatch Fault Zone. 1500. US Geological Survey Professional Paper, Assessment of regional earthquake hazards and risk along the Wasatch Front, Utah, pp. 72.
McCalpin, James P., 2009. Paleoseismology. Vol. 95 Academic press.
Monod, Bernard, Dhont, Damien, Hervouët, Yves, 2010. Orogenic float of the Venezuelan Andes. Tectonophysics 490 (1–2), 123–135. https://doi.org/10.1016/j.tecto.2010.04.036.
Moratto, Z.M., Broxton, M.J., Beyer, R.A., Lundy, M., Husmann, K., 2010. Ames stereo pipeline, NASA's open source automated stereogrammetry software. In: Lunar and Planetary Science Conference. Vol. 41. pp. 2364. http://adsabs.harvard.edu/abs/2010LPI....41.2364M.
Nelson, Alan R., Lowe, Mike, Personius, Stephen, Bradley, Lee-Ann, Forman, Steven L., Klauk, Robert, Garr, John, 2006. Holocene earthquake history of the Northern Weber segment of the Wasatch Fault Zone, Utah. Paleoseismology of Utah 13, 05–08.
Nevado, Fernando, 2012. Integracion Geologica de La Region Moroturo -Palmasola, Estado Yaracuy y Lara, Venezuela. Trabajo especial de grado. Caracas: Universidad Central de Caracas, Facultad de Ingenieria. Escuela de Geologia, Minas y Geofisica.
Palme, Christl, Morandi, M., Choy, J., 2005. Re-Evaluación de Las Intensidades de Los Grandes Sismos Históricos de La Región de La Cordillera de Mérida Utilizando El Método de Bakun & Wentworth. no. 1. Revista Geográfica Venezolana, pp. 233–253.
Pennington, Wayne D., 1981. Subduction of the Eastern Panama basin and seismotectonics of Northwestern South America. J. Geophys. Res. Solid Earth 86 (B11), 10753–10770. https://doi.org/10.1029/JB086iB11p10753.
Pérez, Omar J., Bilham, R., Sequera, M., 2011. GPS derived velocity field in Western Venezuela: dextral shear component associated to the Boconó Fault and convergent component normal to the Andes. Interciencia 26 (2), 69–74.
Pousse-Beltran, Lea, Vassallo, Riccardo, Audemard, Franck, Jouanne, François, Carcaillet, Julien, Pathier, Erwan, Volat, Matthieu, 2017. Pleistocene slip rates on the Boconó fault along the North Andean block plate boundary, Venezuela. In: Tectonics. 2016TC004305https://doi.org/10.1002/2016TC004305.
Reimer, Paula, 2013. IntCal13 and Marine13 radiocarbon age calibration curves 0–50,000 years Cal BP. Radiocarbon 55 (4), 1869–1887. https://doi.org/10.2458/azu_js_rc.55.16947.
Reinoza, Carlos Eduardo, 2014. Application de La Géodésie Satellitaire GNSS à Haute Résolution à La Déformation de La Marge Sud-Caraïbe. Implication Pour l'aléa

Sismique Dans l'Ouest et Le Nord-Est Du Venezuela (PhD thesis). Université Joseph Fourier/Université de Savoie Mont - Blanc, Chambéry.
Rod, Emile, 1956. Strike-slip faults of Northern Venezuela. Bull. Am. Assoc. Pet. Geol. 40, 457–476.
Rodriguez, J.A., Audemard, Franck, 1997. "Estudio Neotectónico y Geología de Fallas Activas En El Piedemonte Surandino de Los Andes Venezolanos (Proyecto INTEVEP 95-061)." Informe Inédito Para INTEVEP, S.A. pp. 1997.
Salgado-Labouriau, Maria Lea, Schubert, Carlos, Valastro Jr., Sam, 1977. Paleoecologic analysis of a Late-Quaternary terrace from Mucubaji, Venezuelan Andes. J. Biogeogr. 4 (4), 313–325. https://doi.org/10.2307/3038190.
Schaetzl, Randall J., Anderson, Sharon, 2005. Soils: Genesis and Geomorphology. Cambridge University Press.
Schubert, Carlos, 1974. Late Pleistocene Mérida Glaciation, Venezuelan Andes. Boreas 3 (4), 147–151. https://doi.org/10.1111/j.1502-3885.1974.tb00673.x.
Silva, Martinez, Sor, Franck Audemard, Guzman, Alejandra Leal, 2016. Un Terremoto Indocumentado. El Misterioso Sismo de 1736 En El Centro Occidente Venezolano. 9 (1). Revista Nuestro Sur. Historia, Memoria y Patrimonio, pp. 160–182.
Singer, A., Beltran, C., 1996. Active faulting in the Southern Venezuelan Andes and Colombian Borderland. In: 3rd International Symposium on Andean Geodynamics, pp. 243–246 (Saint – Malo).
Soulas, J.P., 1986. Neotectónica y tectónica den Venezuela. In: 6° Congreso Geológico Venezolano, Memorias. 10. pp. 6639–6656 (Caracas, Venezuela).
Symithe, S., Calais, E., de Chabalier, J.B., Robertson, R., Higgins, M., 2015. Current block motions and strain accumulation on active faults in the Caribbean. J. Geophys. Res. Solid Earth 120 (5). https://doi.org/10.1002/2014JB011779. (2014JB011779).
Trenkamp, R., Kellogg, J.N., Freymueller, J.T., Mora, H.P., 2002. Wide plate margin deformation, Southern Central America and northwestern South America, CASA GPS observations. J. S. Am. Earth Sci. 15 (2), 157–171. https://doi.org/10.1016/S0895-9811(02)00018-4.
Wesnousky, Steven G., Aranguren, Reina, Rengifo, Martin, Owen, Lewis A., Caffee, Marc W., Murari, Madhav Krishna, Pérez, Omar J., 2012. Toward quantifying geomorphic rates of crustal displacement, landscape development, and the age of glaciation in the Venezuelan Andes. Geomorphology 141–142 (March), 99–113. https://doi.org/10.1016/j.geomorph.2011.12.028.